# 3-D Triangulation of a Sun-grazing Comet

W. T. Thompson

*Adnet Systems Inc., NASA Goddard Space Flight Center*

*Code 671, Greenbelt, MD 20771*

`William.T.Thompson@nasa.gov`

## ABSTRACT

The bright Kreutz comet C/2007 L3 (SOHO) entered the fields of view of the twin *Solar Terrestrial Relations Observatory* (STEREO) COR1 telescopes on 7–8 June 2007. The 12° separation between the two spacecraft at the time afforded the opportunity to derive the position of the comet's tail in three-dimensional space using direct triangulation. The track of the comet's orbit is compared against more traditional orbital calculations using observations from the STEREO COR2 telescopes, and from the Large Angle and Spectrometric Coronagraph (LASCO) aboard the *Solar and Heliospheric Observatory* (SOHO). The shape of the comet's tail shows that it is composed of dust particles released when the comet was between 18 and 22 solar radii, with no significant dust production after that. The comet did not survive perihelion passage, but a rare faint remnant of the comet tail persisted for several hours after the break-up, and was seen by both the SOHO and STEREO coronagraphs to drift slowly away from the Sun. This tail remnant was found to be composed of particles far back from the head of the comet. The motion of the tail remnant shows a loss of angular momentum during the passage through the solar corona. Atmospheric drag is estimated to account for a significant fraction of this change in angular momentum, but indications are that other mechanisms may be required to completely account for the total amount of change.

*Subject headings:* Comets, dynamics; Data reduction techniques

## 1.   Introduction

It has long been known that some comets, called "sungrazers", have orbits whose perihelion passages take them very close to the solar surface (Marsden 2005). The number of known sungrazer comets increased dramatically with the advent of space-based coronagraphs, starting with the discovery of about 15 comets in the *Solwind* and *Solar Maximum Mission* (SMM) coronagraph data (Marsden 1989), and continuing with the discovery of close to 1500 comets to date by the *Solar and Heliospheric Observatory* (SOHO) (Biesecker *et al.* 2002). The vast majority of these

comets have very similar orbital parameters, and are collectively known as the Kreutz group (see references above).

The *Solar Terrestrial Relations Observatory* (STEREO) mission consists of two spacecraft in independent heliocentric orbits designed to give a stereo view of the Sun (Kaiser *et al.* 2008). The Sun Earth Connection Coronal and Heliospheric Investigation (SECCHI) instrument suite includes coronagraphs similar to those of SOHO (Howard *et al.* 2008). The outer coronagraph, COR2, observes a similar regime to that of the SOHO C2 and C3 telescopes, from 2.5–15 $R_\odot$ (solar radii), while the inner coronagraph, COR1, observes from 1.4–4 $R_\odot$. The addition of viewpoints off the Sun-Earth line provides a new tool for studying sungrazing comets and their orbits. Much work has already been done on the use of the COR2 telescopes and the SECCHI Heliospheric Imager to improve the orbital determinations of Kreutz comets (K. Battams, private communication); here we concentrate on the observation of sungrazer comets by the inner coronagraph COR1 to demonstrate how 3D triangulation techniques can be used to explore the dynamics of comet tails.

According to Biesecker *et al.* (2002), most Kreutz sungrazing comets peak in brightness between 11–12 $R_\odot$, and then fade as they approach the Sun. Few comets are observed at heliocentric distances closer than 7 $R_\odot$, but when they are, the fading tends to stop at $\sim 7 R_\odot$. Based on these results, one would expect that only a few sungrazing comets would survive to enter the COR1 field of view. As of this writing, three comets have been observed by COR1, on 7-8 June 2007 (C/2007 L3), 23 May 2008 (C/2008 K4), and 16 June 2008 (C/2008 L14). This paper reports on the COR1 observations of the first of these comets. An unusual feature of this comet is that a faint remnant of the tail was seen to drift slowly away from the Sun few several hours after perihelion. The properties of this tail remnant are discussed in Section 6.

## 2. The comet C/2007 L3 (SOHO)

A bright Kreutz sungrazing comet was seen by the SOHO and STEREO coronagraphs as it passed by the Sun in early June 2007. Designated C/2007 L3 (SOHO), the comet reached perihelion on June 8, around 5:30 UT. We report here on observations of this comet by the STEREO COR1 coronagraphs, which made the observations of the comet which were closest to the Sun, between 1.4 and 4 apparent solar radii. The comet entered the COR1-B (Behind) field of view at 23:16 UT on June 7th, and that of COR1-A (Ahead) the next day at 2:55 UT. From that point onward, until the comet broke up, it was visible in both spacecraft (Fig. 1). The angular separation of the two spacecraft at that point in the mission was just under 12°, providing an excellent opportunity to explore the comet tail dynamics with stereoscopic techniques.

The different perspectives of the two STEREO spacecraft affect the appearance of the comet in the two COR1 views. The comet appears closer to the Sun as seen by COR1-B, and the orientation of the tail is more inclined. This is because the comet is approaching from behind the Sun, and is more foreshortened in the Behind view, while the Ahead spacecraft sees the comet tail more from

Behind                    Ahead



2007−06−08 03:25
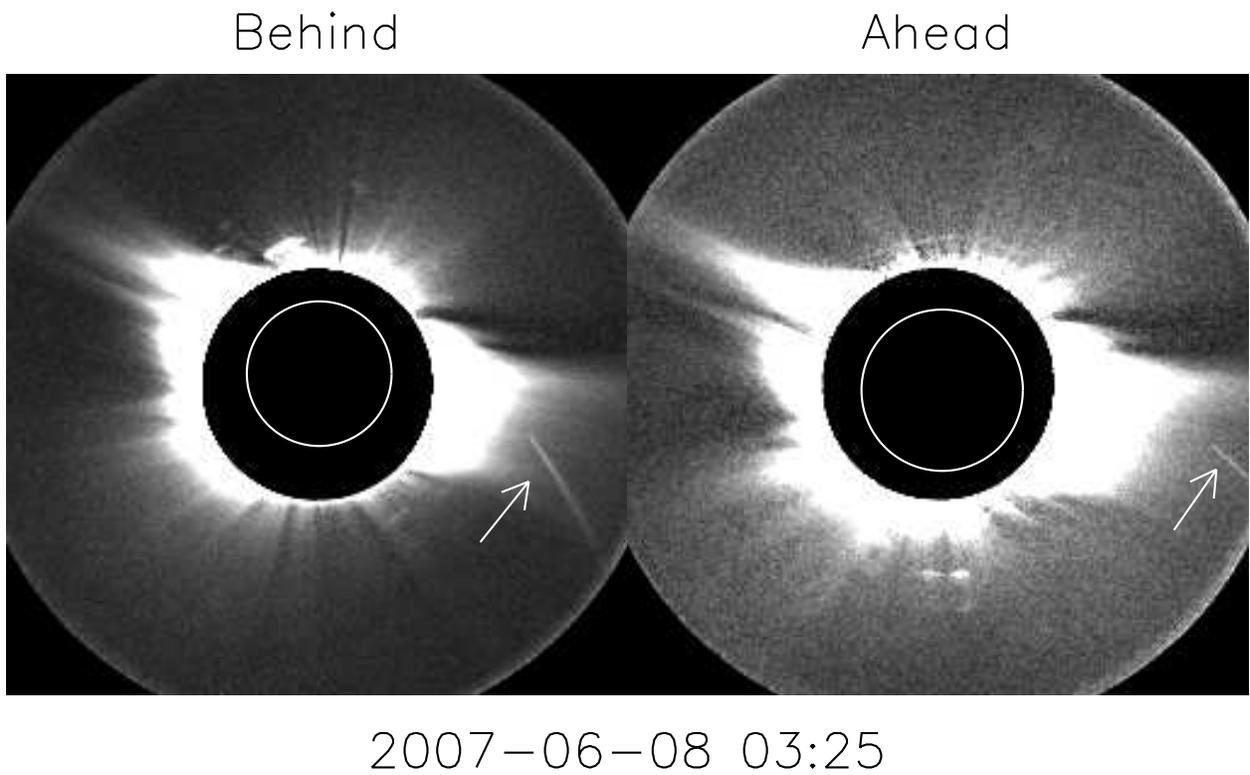
Fig. 1.— The sungrazer comet as seen by the two STEREO COR1 telescopes. The circles represent the position of the Sun behind the occulters.

the side. This also makes the comet appear brighter in the Behind view, since the optical depth is higher. Fig. 2 shows a close-up view of the comet. The appearance is very typical of a sungrazing comet, with a narrow tail following an almost straight line from the comet head. No polarized brightness signal could be detected. As the comet gets closer to the Sun, the tail gets fainter and broader. In particular, the head of the comet becomes less distinct and harder to make out.

## 3. Measurement technique

In order to measure the coordinates of a feature in the COR1 images using triangulation, one must know the positions of the two STEREO spacecraft, the location of the Sun behind the COR1 occulters, and the image orientation. The spacecraft positions are derived from ephemeris files delivered by the project in "SPICE" format (Eichstedt and Thompson 2008). Knowledge of the COR1 pointing is based on boresight data from the SECCHI Guide Telescope, and roll data from the spacecraft attitude history files, as described in Thompson and Reginald (2008). In that work, the coalignment accuracy was determined to be in the range of 7.5 to 15 arcseconds (1–2 pixels) by comparing triangulation measurements of the planet Mercury against ephemeris values.

We used the IDL routine `scc_measure` in SolarSoft to trace out the path of the comet tail in 3D space. The action of this program is as follows: The user is presented with two side-by-side images, one from each of the two STEREO spacecraft. The images are selected so that they represent the same observation time, with a slight offset to account for the difference in light travel time from the Sun. The user can zoom in on the region of interest in the two images, and adjust the color table and data range to optimize the appearance of the feature being measured. A point is selected on one image with the cursor. The program calculates the three-dimensional line of sight represented by this point, and then overplots the projection of this line onto the image from the other satellite. This is known as an epipolar line. Since the COR1 optics produce a gnomonic projection on the CCD detector, straight lines in space will always appear as straight lines in the image. The feature selected by the user in the first image must appear along the epipolar line drawn by the program in the second image. The correct location along this line is selected by the user, which leads to another line of sight calculation which intersects the original line of sight. The intersection of these two lines determines the 3D location of the feature.

The concept behind the epipolar geometry used by `scc_measure` is demonstrated in Fig. 3. The point marked "X" represents the feature of interest, and the solid line from the Behind spacecraft through X represents the measured direction of this feature as seen from Behind, selected by clicking on the Behind image. If this line were physically present in space, it would appear as a single point in the Behind telescope, which would see it edge-on. However, it would cut across the image seen by Ahead, and would pass through the feature "X". This is what is meant by the term epipolar line. The inset images in Fig. 3 show the selected point (the head of the comet) in the Behind image, and the resulting epipolar line in the Ahead image. By measuring the direction of the feature as seen by Ahead, represented by the dashed line in Fig. 3, one can then triangulate the position of

Fig. 2.— Close-up view of the sungrazer comet as seen from COR1-B.

"X" as the intersection of the solid and dashed lines.

The comet tail is faint compared to the corona. Therefore, good background subtraction is necessary to ensure that the comet can be distinguished from the corona. Several background subtraction techniques were used to analyze the data. It was found that different methods worked best depending on the distance from the Sun and the width of the portion of the tail being measured. The first technique used was to derive a background from an examination of the five images surrounding the image in question, i.e. the two previous images, the two following images, and including the image in question. For each pixel position, the corresponding value in each image was examined to find the minimum value over the five images. The background image was thus the collection of pixel-by-pixel minima. This technique was most effective at suppressing the background corona surrounding the comet, and was used for the bulk of the data. However, as the tail became broader and weaker, this technique became less effective, because the broad parts of the tail would be partially suppressed as background. For these later data, a single background image was derived, formed as the minimum over the entire time range being analyzed. In addition, a $5 \times 5$ boxcar smoothing was applied to these later data to reduce the noise.

The image of the comet tail is clearest in the Behind images. It was found that the best results were obtained by first selecting a point along the fainter comet tail in the COR1-A image. The intersection of the resulting epipolar line with the clear comet tail image from Behind could then be easily determined. Cursor selections were targeted for the apparent center of the tail at each point along its length for the most consistent data. No attempt was made to find the tail edges or to measure the width of the tail. This procedure was repeated at each time step to build up a series of traces of the comet tail.

The resulting traces are shown in Figs. 4 and 5. The coordinate system used to display these data is explained in Section 4. The motion of the comet is from left to right. Asterisks mark the position of the comet head. The last few traces could not be carried all the way to the head, because of interference from bright coronal streamers. The measurement of the other end of the tail is limited by the edge of the COR1-A field of view. The highest quality data are the earliest traces. As the comet approached the Sun, the tail became broader and fainter, and thus harder to measure.

## 4. Orbital parameters

The starting points of the first nine traces in Figs. 4 and 5 were fitted to derive the orbital parameters of the comet. The remaining five head positions were judged to be of lower quality, and were omitted from the fit. The results are shown in Table 1. These parameters were used to define an orbital plane for the comet. The data in Figs. 4 and 5 are plotted in this plane, with Earth constrained to the $x$-$z$ plane, at an angle of -33°6 to the $+x$ axis.

Also shown in Table 1 are orbital parameters derived from SOHO observations alone (Zhou
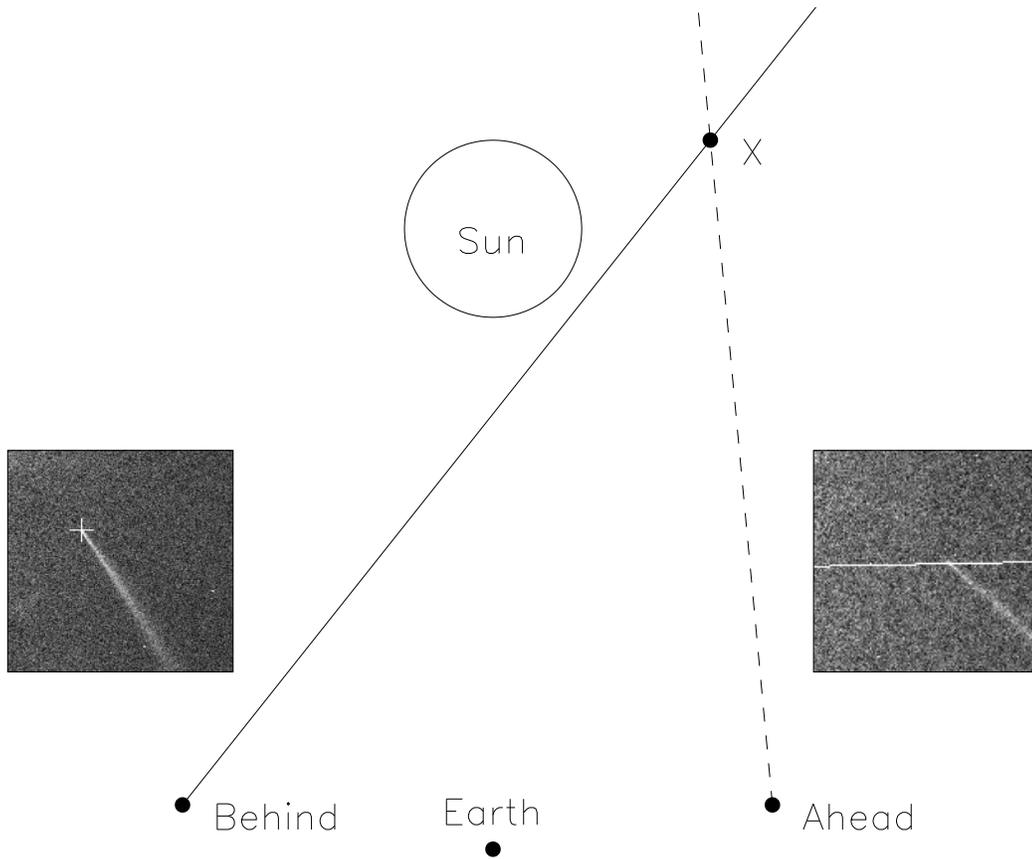
Fig. 3.— Demonstration of the epipolar geometry used to measure the position of the comet in three-dimensional space. See text for details. The inset images show the selected point in the Behind image, and the resulting epipolar line in Ahead.

Table 1. Orbital parameters derived from COR1 triangulation measurements, compared against measurements made using SOHO data, and a combination of SOHO and STEREO COR2 and HI1 data.

|  | COR1 | SOHO | SOHO+STEREO |
|---|---|---|---|
| Perihelion distance (AU) | 0.0070 | 0.0071 | 0.00712 |
| Perihelion time (2007-06-08) | 05:35 | 05:31 | 05:27 |
| Eccentricity (assumed) | 1 | 1 | 1 |
| Inclination (°) | 144.57 | 144.60 | 144.542 |
| Longitude of ascending node (°) | 5.94 | 4.45 | 4.824 |
| Argument of periapsis (°) | 85.26 | 83.48 | 83.803 |
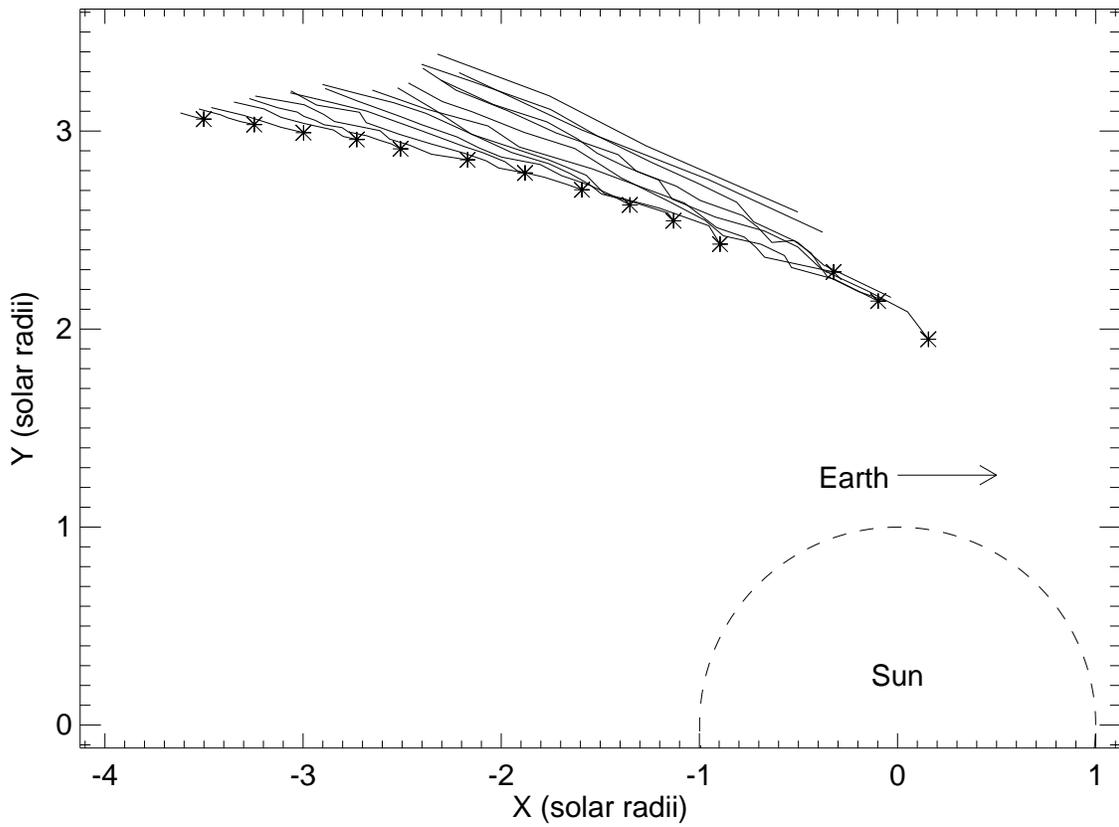
Fig. 4.— Traces of the comet tail, viewed from above the plane of the comet's orbit. Each trace represents a different time of observation. Asterisks mark the comet head. The last few traces do not extend all the way to the head. The comet moves from left to right in this plot. An expanded view of the same data is shown in Fig. 5.
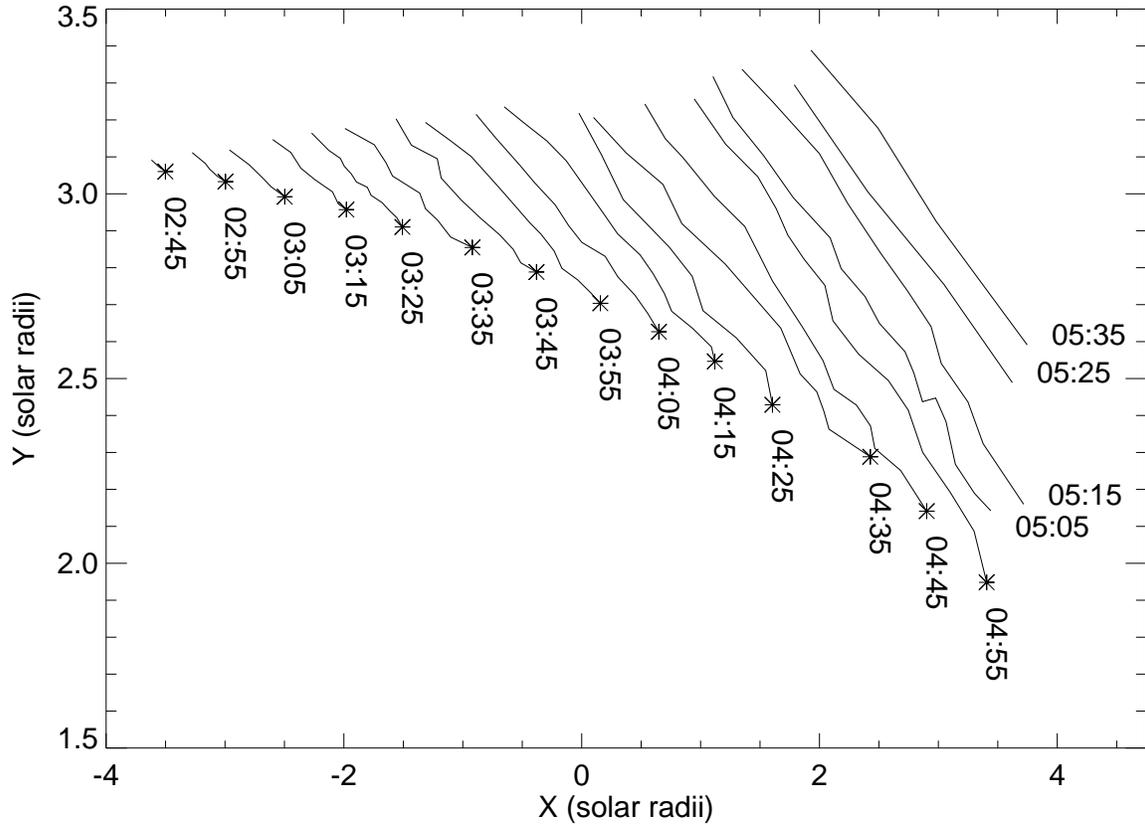
Fig. 5.— Same data as in Fig. 4, but with an extra 0.25 solar radii added to each successive trace in the horizontal direction, and with unequal scaling along the $x$ and $y$ axes, to better distinguish the traces. Only the leftmost trace is plotted at the correct position. Each trace is marked with the observation time, as seen by COR1-A.

*et al.* 2007), and from a combination of SOHO measurements and STEREO HI1 and COR2 measurements (Battams and Marsden 2008). In general, there is good agreement between the three sets of parameters. The highest accuracy is achieved by combining the SOHO and STEREO measurements together. The COR1 measurements cover only a short portion of the comet's orbit, and do not include nearby stars as references, as can be done with the larger coronagraphs. Therefore, the parameters derived from the COR1 observations alone are not expected to be of as high quality as those derived using more traditional techniques. However, the close agreement in Table 1 validates the COR1 triangulation measurements of the comet tail.

Note that the orbital parameters derived from the COR1 trigonometric measurements do not contain any assumptions other than the approximation that the orbit is parabolic ($e = 1$). Sungrazing comet observations from earlier space missions generally required additional assumptions to derive an orbital solution. MacQueen and Cyr (1991) pointed out that it was impossible from the SMM comet observations to distinguish between prograde or retrograde motions. Marsden (1989) assumed Kreutz $L$ and $B$ parameters (longitude and latitude of perihelion) for the SMM and *Solwind* comets in order to fit the orbits. Position measurements for sungrazing comets improved with the SOHO mission (Marsden 2005). However, Kreutz parameters were still used as a starting point for the reiterative orbital solutions for most of the SOHO comets (Biesecker *et al.* 2002). The same technique can be used with STEREO data, with the two views acting together to refine the parameters. However, such assumptions are not required with the STEREO measurements. Simultaneous measurements from two viewpoints removes any ambiguity in the orbital solution.

## 5. Tail dynamics

One can see from Fig. 4 that the tail mainly follows the orbit of the comet, with only a small amount of drift radially outward. Thus, one can conclude that this is a dust tail rather than an ion tail. We applied the standard syndyne/synchrone analysis (Finson and Probstein 1968) to the shape of the comet tail. A *syndyne* (or *syndyname*) is a curve of points calculated assuming dust particles are emitted continuously with a constant value $\beta$ of the radiation pressure to gravitational attraction (sometimes written as $1 - \mu$). Since both radiation pressure and gravity obey the $1/r^2$ law, the dust particles follow trajectories as if acted upon by a gravity weakened by the factor $\mu = 1 - \beta$. A *synchrone* is a curve calculated assuming dust particles are emitted with a wide variety of $\beta$ values, but at a single time $t$. Sekanina (2000) studied 11 sungrazing comets observed by SOHO, and concluded that the tail shapes did not match the syndyne relationship, but were best fitted as synchrone curves with dust production ending when the comet's orbit brought it within 20–30 $R_\odot$. We find the same behavior for comet C/2007 L3. The tail shapes do not curve outward like a syndyne, but instead go straight back from the head. The shape is best characterized by a synchrone with a time of emission between 18 and 24 hours before perihelion, when the heliocentric distance was between 18 and 22 $R_\odot$. This relationship held for all the pre-perihelion traces shown in Figs. 4 and 5. A sample syndyne/synchrone plot is shown in Fig. 6. Note that the estimation of

emission 18–24 hours before perihelion does not rest on a single trace, but from an examination of all the traces leading up to perihelion passage.

An interesting question is whether the dust particles in the comet tail experience any non-radial accelerations. This would be detectable as an elevation of the tail above or below the plane of the comet's orbit. Horanyi and Mendis (1991) discuss the process of grain charging for cometary dust, and predict that the grains will experience electrodynamic forces comparable to, or even larger than, the radiation pressure force. These effects should be particularly strong for sungrazing comets close to the Sun, where $\mathbf{v} \times \mathbf{B}$ is large. However, previous observations of sungrazing comets during orbit-plane transits show no evidence for motion perpendicular to the orbital plane (Sekanina 2000).

The 3D triangulation technique applied to the comet tail allows one to trace the elevation of the comet tail above or below the plane of the comet's orbit without depending on observing from within the orbital plane. The results are shown in Fig. 7. We looked hard for evidence of any non-radial accelerations in the tail. Multiple measurements were made to determine what features were repeatable, and what effect noise had on the data. In the end it was concluded that there was no evidence for motion out of the plane in the pre-perihelion data. The data in Fig. 7 are consistent with the tail being restricted to the comet's orbital plane. The highest quality data are the earliest traces, when the tail was narrow and bright. As the comet approaches the Sun, the tail becomes broader and fainter, and the measurements are correspondingly noisier. However, even for these noisier data, the tail stays within the orbital plane. If we consider the acceleration to be acting over the 18+ hours between particle emission and perihelion, the largest average perpendicular acceleration that is consistent with the data is $\sim$0.03 m s$^{-2}$, while the gravitational acceleration varies between 0.8 and at least 30 m s$^{-2}$ during the same period. Thus, any forces acting perpendicular to the orbital plane are small compared to the other forces acting on the tail particles.

## 6. Faint tail after perihelion

Like all sungrazers so far observed from space, the comet broke up as it approached perihelion. However, a faint remnant of the comet tail persisted for some time after the break-up, and was seen by both the SOHO and STEREO coronagraphs to drift slowly away from the Sun. An image of this faint tail as seen by COR1-A is shown in Fig. 8. Such tail remnants are very rare. Marsden (2005) remarks that the tail of the first comet observed by *Solwind*, C/1979 Q1, was still quite evident for 100 minutes after perihelion, and that cometary material diffused around much of the Sun for several hours more (Michels *et al.* 1982), and that faint emissions of Si$^+$ and Ni$^+$ were possibly seen some ten hours after perihelion (Chocol *et al.* 1983). A faint tail remnant was seen following the perihelion passage of comet C/1998 K10 (SOHO), in a manner very similar to that observed by COR1 for C/2007 L3 (D. Biesecker, private communication). It is probable that a few other SOHO comets have shown similar phenomena, but have gone unremarked.
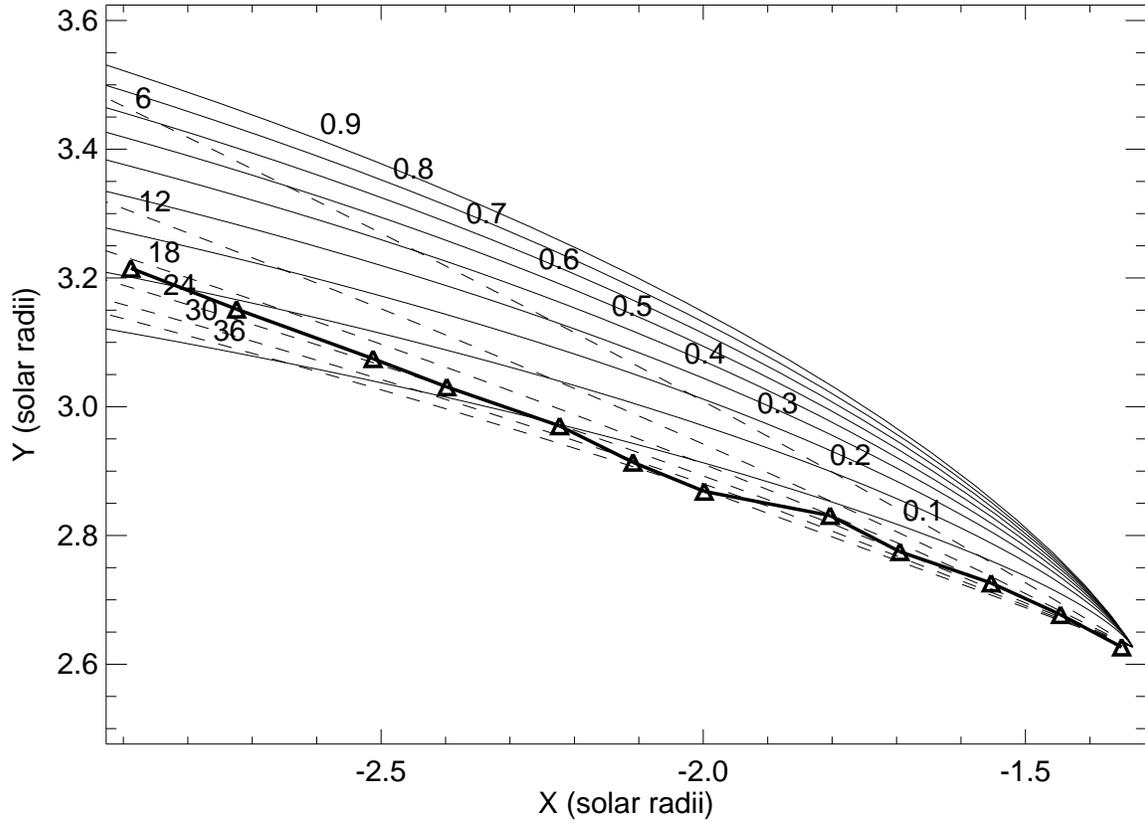
Fig. 6.— Representative syndyne/synchrone curves for the pre-perihelion comet tail. The bold line with the triangle symbols traces out the path of the comet tail. The solid curves represent syndynes with values of $\beta$ running from 0.1 to 0.9, while the dashed curves represent synchrones with emission times $t$ running from 6 to 36 hours before perihelion.
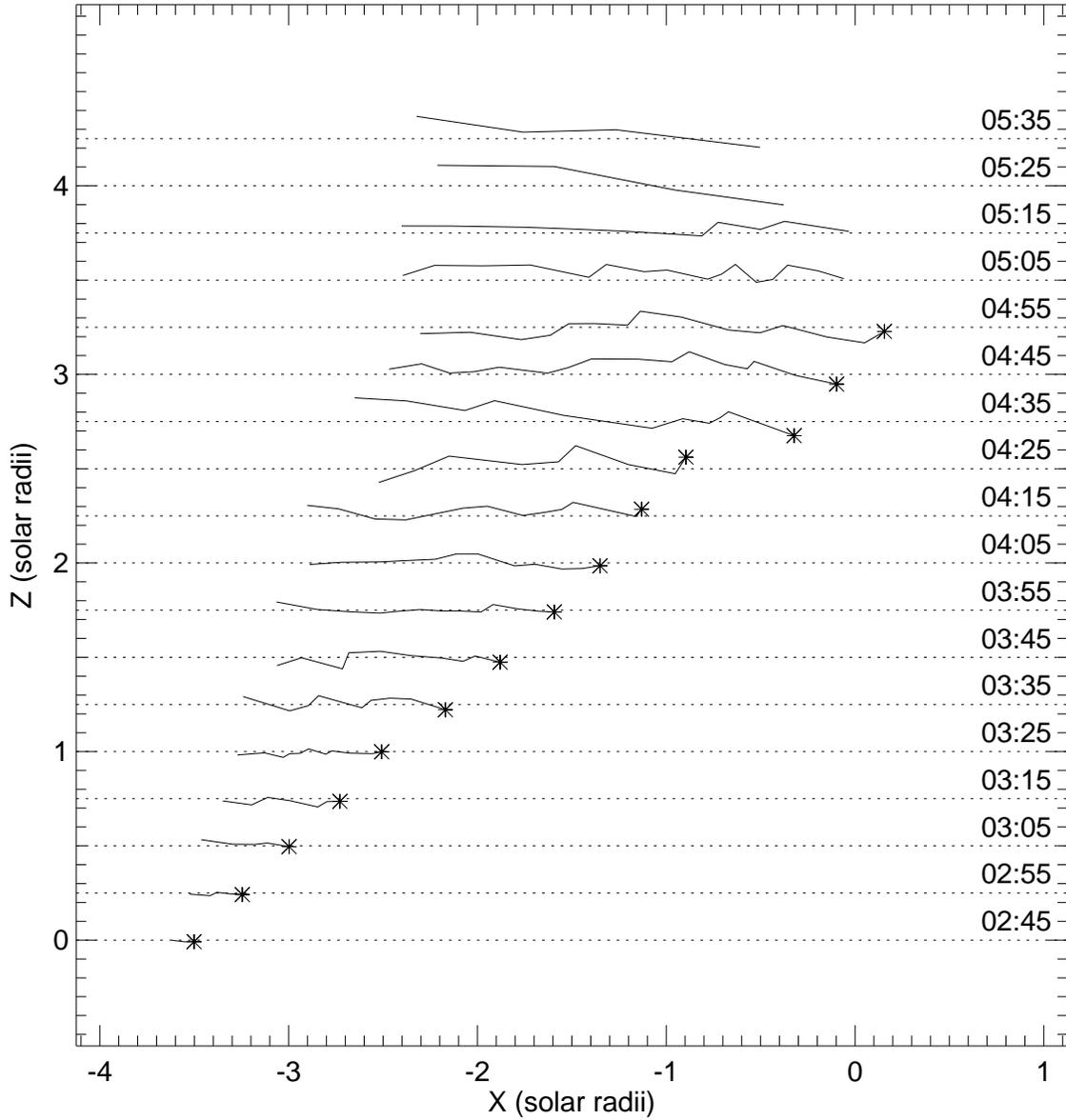
Fig. 7.— Extent of the comet tail above or below the plane of the comet's orbit. An extra 0.25 solar radii has been added to each successive trace in the vertical direction to separate it from its neighbors. Only the bottom trace is plotted at the correct position. Time moves from bottom to top in this plot. The dashed lines represent the position of the orbital plane for each trace.
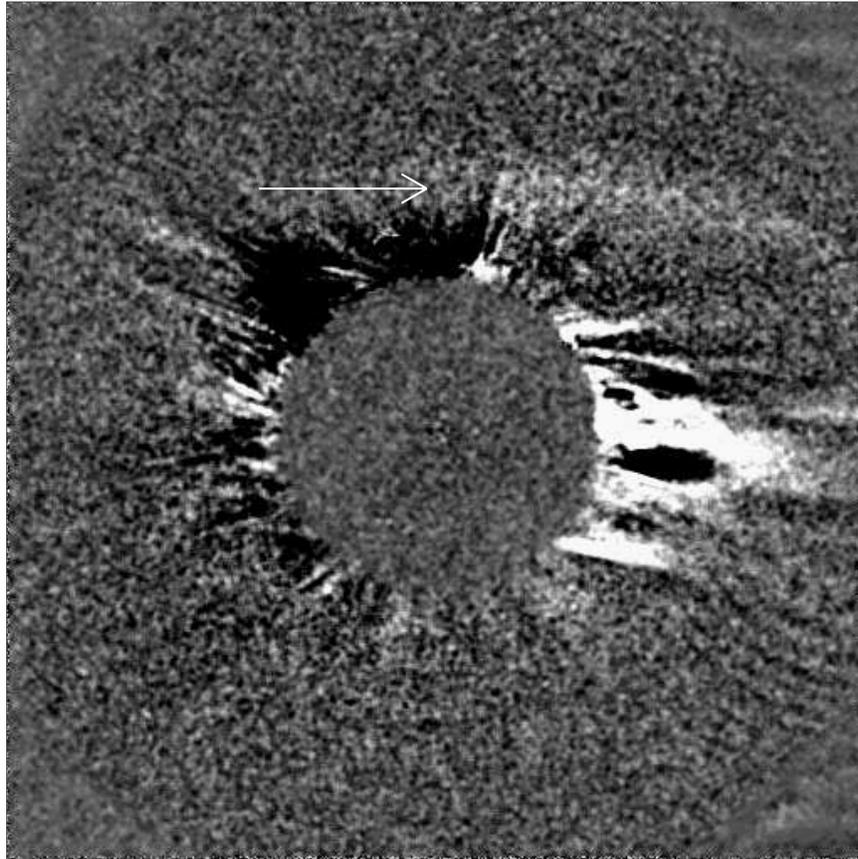
Fig. 8.— Faint remnant of comet tail seen drifting away from Sun after perihelion passage. Most of the background corona is suppressed to bring out the tail.

Because the tail remnant was mostly horizontal in the COR1 images, it was no longer possible to use triangulation to derive three-dimensional positions. Instead, we measured the position of the comet tail on the COR1-A images, where the tail was most evident, and then projected those measurements onto the plane of the comet's orbit. The results are shown in Fig. 9. Every seventh trace is plotted in bold to better demonstrate the movement of the tail remnant.

An important question is whether the tail remnant particles seen after perihelion can be matched to the tail particles seen before perihelion. We applied the same syndyne/synchrone analysis used for the pre-perihelion data to the traces of the faint tail remnant after perihelion. Initially, the results were highly consistent with the earlier results. The shape matched that of a synchrone with a release time 18–24 hours before perihelion. A representative early trace is shown in Fig. 10. However, note that the inferred $\beta$ values are very high, above $\beta = 0.5$. Also, the azimuthal separation between the tail remnant measurements and the extrapolated position of the comet head along its original orbit exceeds 120°. Together, these imply that the remnant consists of particles from far back in the original comet tail.

As time goes on, the tail remnant continues to maintain a synchrone orientation, but the inferred time of emission gradually shifts to earlier times. One possibility we considered was that we were indeed seeing particles emitted at earlier points in the comet's orbit as a function of observation time. It could be that the changing viewing geometry selected out different parts of the tail at different times, with some particles disappearing and other particles appearing as time passed. However, this does not seem to be a good match to the data. If we were starting to see particles emitted continuously prior to the shutoff of emission at 18–24 hours before perihelion, then we would expect the tail remnant to take on the shape of a syndyne rather than a synchrone. It does not do that; instead, it maintains a synchrone shape throughout the observing period. Also, if the viewing geometry were the important factor in determining the visibility of the tail, we would expect the horizontal position of the tail to remain relatively constant. Instead, the tail drifts slowly from right to left as seen by COR1-A, as one would expect for orbiting dust particles.

A more reasonable interpretation is that the particles making up the tail remnant have encountered forces other than gravity and radiation pressure somewhere in their history, and the syndyne/synchrone analysis is no longer strictly valid. The angular motion of the tail remnant around the Sun is somewhat slower than the syndyne/synchrone analysis predicts. The inference is that the particles have lost angular momentum as they rounded the Sun. We can get a rough approximation of the angular momentum of the tail remnant by following the motion of the center of the traces in Fig. 9 and measuring $r^2\omega$, where $r$ is the radial distance from Sun center, and $\omega$ is the angular speed in radians per second. This gives an angular momentum per unit mass $l = (2.8 \pm 0.3) \times 10^{18}$ cm$^2$ s$^{-1}$. Compare this against the value $l_0 = 5.27 \times 10^{18}$ cm$^2$ s$^{-1}$ for the comet itself, and one can see that almost half of the original angular momentum has been lost.

One possible mechanism for a loss of angular momentum is the drag force exerted as the particles traverse the solar corona. The drag force per unit mass $f_{\rm drag}$ for a spherical dust particle
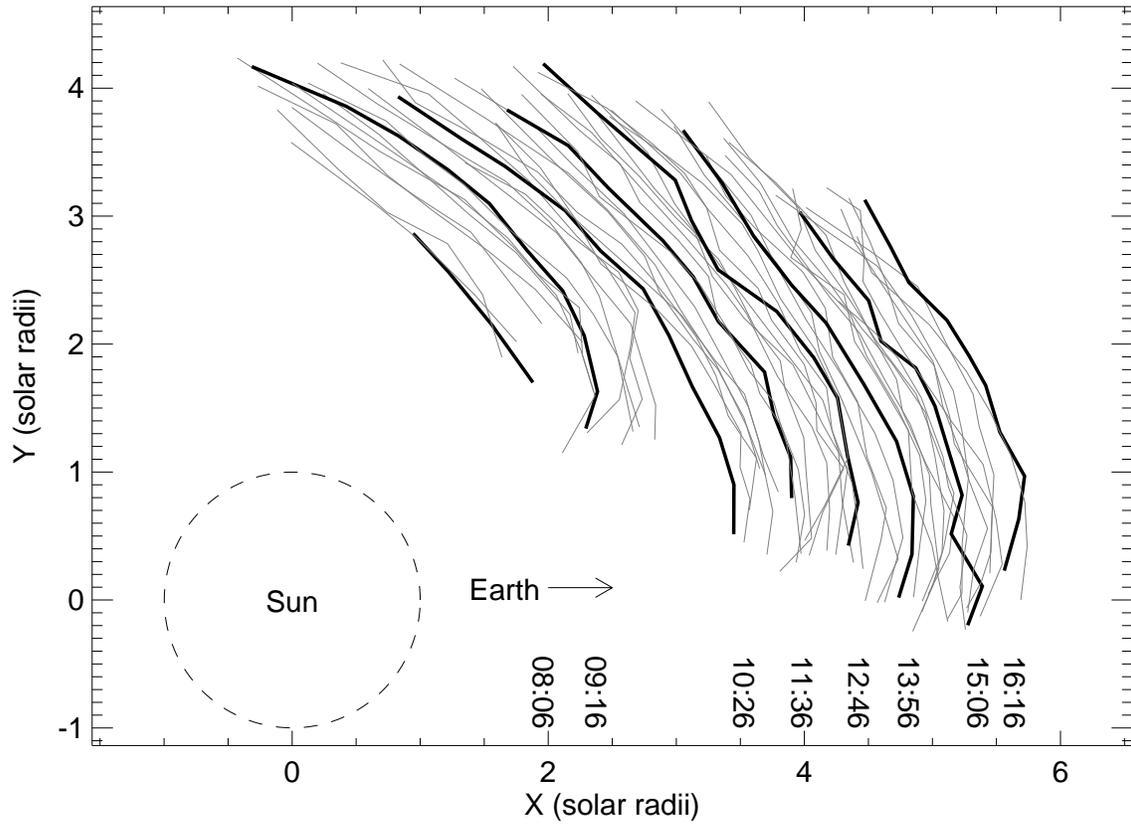
Fig. 9.— Traces of the faint comet tail after perihelion passage. Observation times are given for every seventh trace, marked in bold.
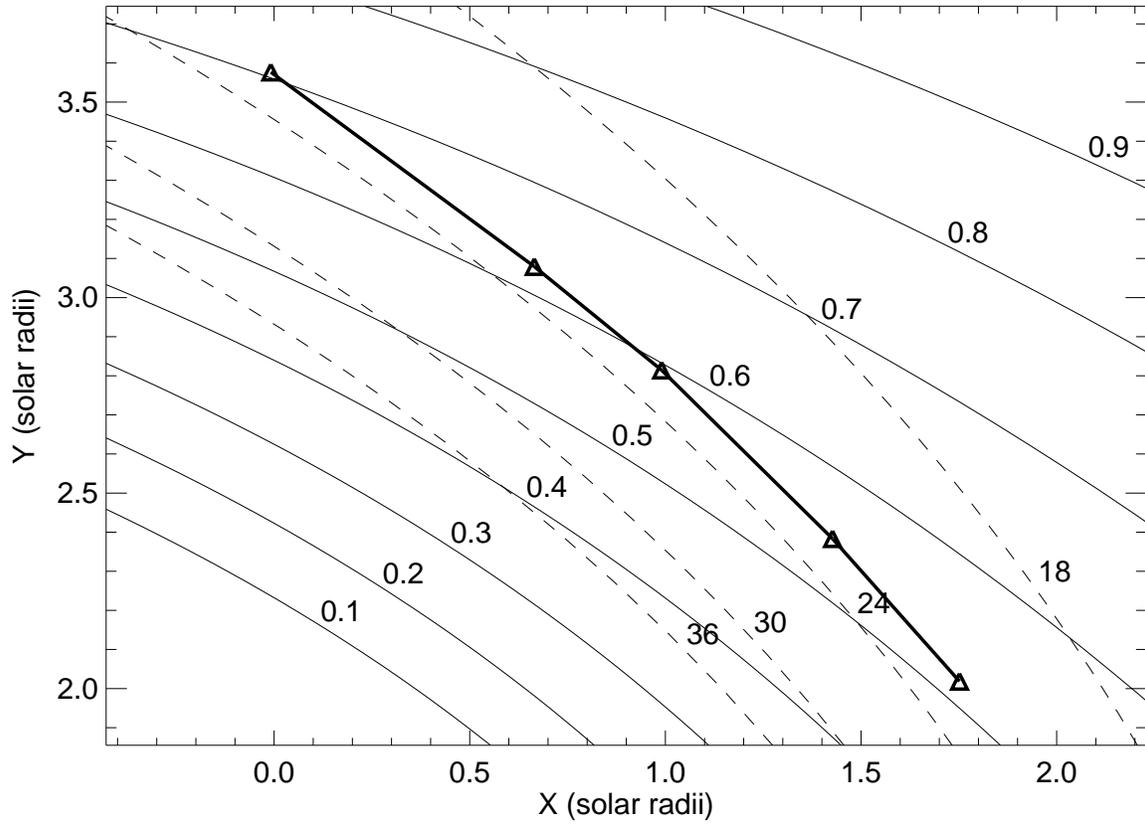
Fig. 10.— Representative syndyne/synchrone curves for the post-perihelion tail remnant. The bold line with the triangle symbols traces out the path of the faint remnant. The solid curves represent syndynes with values of $\beta$ running from 0.1 to 0.9, while the dashed curves represent synchrones with emission times $t$ running from 18 to 36 hours before perihelion. Synchrones for 6 and 12 hours were also calculated, but lay outside this plot.

can be approximated as

$$f_{\mathrm{drag}} = \frac{3v^2\rho}{4a_d\rho_d} \tag{1}$$

where $a_d$ is the particle radius, $v$ is the velocity relative to the coronal material, $\rho$ is the coronal density at the grain's location, and $\rho_d$ is the density of the dust grain. Eq. 1 is for inelastic collisions; for elastic collisions $f_{\mathrm{drag}}$ could be as high as double this value. Fluid dynamic effects are treated as being insignificant at the size scale of a dust particle. To see if drag can account for the loss in angular momentum, we consider the 6 hour period centered on perihelion when the dust particles are at approximately 3 $R_\odot$, and the drag force is acting mostly perpendicular to the radial direction. These values will be used to make an order-of-magnitude estimate of the total change in angular momentum. The coronal density at that location is approximated as $5.6 \times 10^6$ hydrogen atoms per cubic centimeter, based on Table 14.20 of Cox (2000) for a coronal streamer. It is evident from the images that the comet tail is passing through the streamer belt at this time. We adopt $v = 400$ km s$^{-1}$ as a rough vector combination of the orbital speed of the particles and the solar wind speed. Putting all this together, we end up with an estimate for the total change in angular momentum per unit mass of

$$\Delta l = (5 \times 10^{13} \text{ gm s}^{-1})/(a_d\rho_d). \tag{2}$$

One can remove the product $a_d\rho_d$ from Eq. 2 by expressing it as a function of the parameter $\beta$. For spherical dust particles,

$$\beta = \left(\frac{3L_\odot}{16\pi G M_\odot c}\right)\frac{Q}{a_d\rho_d} = K\frac{Q}{a_d\rho_d}, \tag{3}$$

where $L_\odot$ and $M_\odot$ are the solar luminosity and mass respectively, $G$ is the gravitational constant, $c$ is the speed of light, and $Q$ is a dimensionless coupling efficiency. For perfect absorption or isotropic scattering $Q = 1$, while $Q = 2$ for perfect reflection back towards the Sun. The expectation is that $Q$ should be close to unity. The constants inside the brackets of Eq. 3 can be combined into a single constant $K = 5.88 \times 10^{-5}$ g cm$^{-2}$. Thus, Eq. 2 can be recast as

$$\Delta l = (8.6 \times 10^{17} \text{ cm}^2 \text{ s}^{-1})(\beta/Q). \tag{4}$$

Fig. 10 implies that $\beta = 0.6$. In fact, we cannot directly ascertain $\beta$ because the post-perihelion dust particles no longer strictly follow the synchrone/syndyne relationship. However, $\beta = 0.6$ is a good assumption for particles this far back in the tail, and we will adopt this value. Thus, we would need a rather low value of $Q = 0.2$ to match the change of $\sim$2.5 $\times 10^{18}$ cm$^2$ s$^{-1}$ seen in the data. Given that we expect $Q$ to be close to unity, this means that the estimated amount of atmospheric drag can account for about 20% of the total change in angular momentum. Therefore, although this is a rather rough calculation, and there are a number of factors which could increase the calculated drag effect, this low value of $Q$ implies that other mechanisms may also be contributing to the observed change in angular momentum.

## 7. Conclusions

We have demonstrated that observations from multiple simultaneous viewpoints can be used to study the tail dynamics of sungrazing comets. In particular, we can study the tail dynamics with a full three-dimensional treatment, and look for motions out of the plane of the comet's orbit. Previously, this could only be done when Earth or the spacecraft was passing through the comet's orbital plane. We confirm the results of Sekanina (2000) that the tail shape is best characterized by a synchrone, with the particles making up the tail being released between 18–22 hours before perihelion. No out-of-plane motions were found, implying that electrodynamic forces are not a significant contributor to the dynamics of the dust tail.

The faint tail remnant seen for several hours after perihelion passage was found to be composed of particles far back from the head of the comet. These particles follow orbits which are close to those predicted by the relationship between gravity and radiation pressure, but which have been modified by a loss of angular momentum. Some part of this loss of angular momentum is estimated to be due to atmospheric drag from the solar corona. However, other mechanisms may also be needed to completely account for the total drop in angular momentum.

Michels *et al.* (1982) interpreted the diffuse remnant seen after the perihelion passage of comet C/1979 Q1 as disintegration products being driven out by radiation pressure. The orbital solutions for that comet included paths which may have led to a collision with the solar surface. A particularly strong argument for this interpretation is that projection onto the comet's orbital plane would require distances between 16–43 $R_\odot$. In many ways the behavior of the diffuse glow seen after C/1979 Q1 is quite different from that seen after C/2007 L3. Therefore, we don't dispute the Michels *et al.* interpretation for the 1979 comet. However, the post-perihelion behavior of comet C/1998 K10 is very similar to that of C/2007 L3, and is assumed to be the same phenomenon.

### REFERENCES

Battams, K. and Marsden, B. G. (2008). Comets C/2007 L2, 2007 L3, 2007 L13, 2007 V4 (SOHO). *Minor Planet Electronic Circulars*, **2008-G44**, 44–+.

Biesecker, D. A., Lamy, P., Cyr, O. C. S., Llebaria, A., and Howard, R. A. (2002). Sungrazing comets discovered with the SOHO/LASCO coronagraphs 1996–1998. *Icarus*, **157**, 323–348.

Chocol, D., Rušín, V., Kulčár, L., and Vanýsek, V. (1983). Emission features in the solar corona after the perihelion passage of comet 1979 X1. *Astrophys. Space Sci.*, **91**, 71–77.

Cox, A. N. (2000). *Allen's Astrophysical Quantities*. 4th ed.; New York: AIP Press; Springer.

Eichstedt, J. and Thompson, W. T. (2008). STEREO ground segment, science operations, and data archive. *Space Sci. Rev.*, **136**, 605–626.

Finson, M. L. and Probstein, R. F. (1968). A theory of dust comets. I. Model and equations. *Ap. J.*, **154**, 327–352.

Horanyi, M. and Mendis, D. A. (1991). The electrodynamics of charged dust in the cometary environment. In R. L. Newburn, J., Neugebauer, M., and Rahe, J., editors, *Comets in the post-Halley era, Vol. 2*, pages 1093–1104.

Howard, R. A., Moses, J., Vourlidas, A., Newmark, J., Socker, D., Plunkett, S., Korendyke, C., Cook, J. W., Hurley, A., Davila, J. M., Thompson, W. T., Cyr, O. S., Mentzell, E., Mehalick, K., Lemen, J., Wuelser, J., Duncan, D., Tarbell, T., Wolfson, C., Moore, A., Harrison, R. A., Waltham, N. R., Lang, J., Davis, C., Eyles, C., Mapson-Menard, H., Simnett, G., Halain, J., Defise, J., Mazy, E., Rochus, P., Mercier, R., Ravet, M. F., Delmotte, F., Auchere, F., Delaboudiniere, J., Bothmer, V., Deutsch, W., Wang, D., Rich, N., Cooper, S., Stephens, V., Maahs, G., Baugh, R., and McMullin, D. (2008). Sun Earth Connection Coronal and Heliospheric Investigation (SECCHI). *Space Sci. Rev.*, **136**, 67–115.

Kaiser, M. L., Kucera, T. A., Davila, J. M., Cyr, O. C. S., Guhathakurta, M., and Christian, E. (2008). The STEREO mission: An introduction. *Space Sci. Rev.*, **136**, 5–16.

MacQueen, R. M. and Cyr, O. C. S. (1991). Sungrazing comets observed by the Solar Maximum Mission coronagraph. *Icarus*, **90**, 96–106.

Marsden, B. G. (1989). The sungrazing comet group. II. *Astron. J.*, **98**, 2306–2321.

Marsden, B. G. (2005). Sungrazing comets. *Annu. Rev. Astro. Astrophys.*, **43**, 75–102.

Michels, D. J., Sheeley, N. R., Howard, R. A., and Koonen, M. J. (1982). Observations of a comet on collision course with the sun. *Science*, **215**, 1097–1102.

Sekanina, Z. (2000). Solar and Heliospheric Observatory sungrazing comets with prominent tails: evidence on dust-production peculiarities. *Ap. J.*, **545**, L69–L72.

Thompson, W. T. and Reginald, N. L. (2008). The radiometric and pointing calibration of SECCHI COR1 on STEREO. *Solar Phys.* in press.

Zhou, B., Battams, K., Yuan, S., Watson, A., and Marsden, B. G. (2007). Comets C/2007 L1, 2007 L2, 2007 L3, 2007 L4, 2007 L5 (SOHO). *Minor Planet Electronic Circulars*, **2007-T94**, 94–+.

---